Methods for histological characterization of cryo-induced myocardial infarction in a rat model

Matthew Alonzo [a,b], Monica Delgado [a,b], Carol Cleetus [a,b], Shweta Anil Kumar [a,b], Vikram Thakur [d], Munmun Chattopadhyay [d], Binata Joddar [a,b,c],*

[a] Inspired Materials & Stem-Cell Based Tissue Engineering Laboratory (IMSTEL), The University of Texas at El Paso, El Paso, TX, 79968, USA
[b] Department of Metallurgical, Materials, and Biomedical Engineering, M201 Engineering, The University of Texas at El Paso, 500 W. University Avenue, El Paso, TX, 79968, USA
[c] Border Biomedical Research Center, The University of Texas at El Paso, 500 W. University Avenue, El Paso, TX, 79968, USA
[d] Department of Molecular and Translational Medicine, Center of Emphasis in Diabetes and Metabolism, Texas Tech University Health Sciences Center, 5001 El Paso Drive, El Paso, TX, 79968, USA

ABSTRACT

Ligation of the left anterior descending (LAD) coronary artery has been commonly employed to induce myocardial infarction (MI) in animals; however, it is known to pose setbacks in the form of cardiac arrhythmias and unpredictable areas of necrotic damage. Cryo-infarction is an alternate method that has been adopted to create a reproducible model of a myocardial injury. In this study, Sprague-Dawley rats were subjected to thoracotomy followed by cryo-induced infarction of the heart, while the control-sham group was only subjected to thoracotomy following which the heart was collected from all animals. Tissue sections were stained with hematoxylin and eosin and analyzed to determine cardiac muscle density, fiber length, and fiber curvature. Observations revealed reduced muscle density, cardiac fiber length, and distorted fibers in infarcted tissue sections. Gomori's Trichrome staining was performed on tissue sections to study the effects of post MI on collagen, which showed enhanced intensity of collagen staining indicating fibrosis for the experimental models as compared to the sham models, an established consequence to myocardial injury. Immunohistochemical staining of the tissue sections with DAPI and connexin-43 (Cx-43) revealed that there was reduced DAPI staining and a less pronounced expression of Cx-43 in the experimental samples as compared to the sham samples. Results implied significant cell damage resulting from the cryo-infarction, subsequently disrupting and disaggregating the functional Cx-43 junction in cardiac myocytes, which is essential for normal and healthy cardiac physiology and function. This quantitative histological study of cryo-induced MI in a rat model can aid others attempting to optimize MI models in rats via cryo-injury, to study cardiac disease progression, and to aid in the construction of engineered cardiac tissues.

1. Introduction

Myocardial infarction (MI) is the consequential event that follows the occlusion of the vessels in the myocardium (Choo et al., 2019). Suboptimal perfusion of oxygen-rich blood to the heart's thick muscle wall leads to hypoxia, causing millions of cells to die (Vunjak-Novakovic et al., 2011). In the body's attempt to rebalance homeostasis, inflammation ensues to remove necrotic tissue, and extracellular matrix remodeling occurs through the deposition of a dense collagenous scar (Xue and Jackson, 2015; Richardson et al., 2011). Although helping

restore some function to the organ, over time, the heart must overcompensate for the stiff and non-contractile properties of the scar, eventually leading to heart failure (Rusu et al., 2019).

To help aid with the decreased pumping efficiency of the infarcted heart, numerous research groups worldwide have attempted to engineer cardiac tissues in-vitro that could potentially be used as grafts to replace damaged myocardium following MI. We previously formulated a fibrinogen-gelatin based hydrogel that was fabricated into a mesh-like scaffold via extrusion-based 3D bioprinting (Anil Kumar et al., 2019). The cardiac patch exhibited comparable mechanical properties, oriented

tissue formation, and heterocellular coupling between cardiomyocytes and fibroblasts, as seen in a natural heart (Anil Kumar et al., 2019). Despite the various strides that have been taken in the field of cardiac tissue engineering, there is an urgent need to understand the underlying pathophysiology of MI and the subsequent disease progression (Richardson et al., 2011). Understanding the pathological progression of an MI model will help researchers design better strategies to engineer a cardiac patch.

The histopathological progress of a naturally-occurring MI is well documented and can be used to understand the age of the infarct (Bouchardy and Majno, 1974; Michael C. Fishbein et al., 1978; White et al., 1936). Although literature describes an array of techniques that can be employed to achieve acute coronary occlusion in the experimental animal model, direct ligation of the left anterior descending artery (LAD), which is the largest coronary artery that descends on the anterior interventricular sulcus to the apex, continues to be the most frequently opted method (Schwarzer, 2016). However, LAD ligation has been observed to increase the occurrence of post-operative mortality resulting from the presence of cardiac arrhythmias, bleeding, and pneumothorax (Reichert et al., 2017). In addition, LAD is known to produce random areas of necrotic damage (Ciulla et al., 2004). Moreover, this model has been described as time-consuming and expensive, while facing critiques with regard to animal protection efforts (Klocke et al., 2007).

Cryo-infarction has been investigated as an alternative approach to induce an MI. Although myocardial cryo-damage is significantly different from that caused by ischemia, it results in a standardized injury that replicates cellular patterns consistent with coagulation necrosis, early microvascular reperfusion, hemorrhage, inflammation, reparation, and scarring observed in myocardial infarction eventually leading to heart failure, generating a model that may be suitable to study myocardial injury (Ciulla et al., 2004). Cryo-infarction has also been successfully applied in other studies with very significant outcomes (van den Bos et al., 2005), which prompted us to form the hypothesis that cryo-infarction can lead to an optimized yet easily reproducible model of injury for the induction of MI in a rat model. Although there are numerous citations in the literature describing the usage of mouse models to assess the efficacy of cryo-infraction (van den Bos et al., 2005, Duerr2010), inducing MI in rat hearts using this technique has been unexplored until now, imparting originality to our study. In the last decade, numerous papers have been published on studies performed in animal models of heart failure and hypertrophy, most of which have been performed in rats (Hasenfuss, 1998).Therefore it is essential to induce and optimize the cryo-MI procedure in rats which can eventually lead to establishment of a model for induction of cardiac hypertrophy and heart failure. We have further adopted histological quantification methods, which will provide direction and guidance to other researchers for optimization of an MI model, as mostly qualitative descriptions exist of post-MI tissue sections (Bouchardy and Majno, 1974; Fishbein et al., 1978; White et al., 1936).

2. Materials and methods

2.1. Subjects

For this study, a minimum of n = 6 animals were used for each condition amongst an approved total of 42 animals employed for the entire study, being approved by the IACUC at the University of Texas at El Paso. All animal experiments were executed in accordance with the National Institutes of Health Guide for the Care and Use of Laboratory Animals (Research, 2011). Procedures were additionally reviewed and approved by the Institutional Animal Care and Use Committee at The University of Texas at El Paso. For this study, male and female Sprague Dawley (Hsd: SD) rats (Envigo, Houston, TX) of ~ 8–10 weeks at the time of surgery were randomly separated into a sham group and an experimental group. The experimental group underwent a thoracotomy,

and an infarct was induced using a cryo-probe. The sham group, on the other hand, underwent the thoracotomy but did not undergo cryo-infarction. SD rats were chosen as the experimental model to extend what is known about cryo-infarction in murine species, as literature has reported such procedures being performed in mice (van den Bos et al., 2005, Duerr2010).

2.2. Chemicals

IsoSol (Isoflurane, USP), surgical-grade chlorhexidine solution, and ChlorHex-Q pre-surgical hand scrub was procured from Vedco Inc. in Saint Joseph, Missouri. Lidocaine Hydrochloride Jelly USP, 2%, was purchased from Akorn Inc. in Lake Forrest, Illinois. Ethanol, Gibco 1X phosphate-buffered saline (PBS), Alfa Aesar 4% paraformaldehyde (PFA) was bought from Fisher Scientific in Hampton, New Hampshire. Mayer's Hematoxylin, Alcoholic Eosin, Sucrose, Xylene, Bouin's Fluid, Working Weigert's Iron Hematoxylin Stain, Trichrome stain, Acetic acid, Sodium Borohydrate were all acquired from Sigma Aldrich.

2.3. Surgical preparation

The weight of the rat was documented prior to each trial and used as a parameter for the induction of anesthesia. A Somnosuite® Low-Flow Anesthesia System (Kent Scientific Corporation, Torrington, CT) was used to vaporize and administer isoflurane loaded in a Pressure-Lok Precision Analytical Syringe (Valco Instruments Company Inc., Houston, TX). The specimen was placed in an induction chamber connected to the Somnosuite via clamped rubber tubing to control airflow. Before each trial, the apparatus was calibrated and checked for any leaks. Once the animal was under anesthesia, it was removed from the chamber and placed supine onto a countertop where isoflurane was continued to be administered through a large nose cone (Kent Scientific Corporation). The left thorax and axillary fur of the subject were shaved and wiped with 70 % ethanol.

A Rat Endotracheal Intubation Kit (Kent Scientific Corporation) was used to prevent pneumothorax when the chest cavity is opened during the thoracotomy. The subject was moved to an intubation stand and hung with suture by its upper incisors under a nose cone. A pulse oximeter connected to the Somnosuite was placed on the subject's paw to monitor the oxygen saturation level, and a thermometer placed in the rectum. Using a dental probe, the tongue was manipulated to expose the throat. Lidocaine was swabbed into the animal's mouth to suppress laryngeal spasms during intubation. A 16 G x 2" catheter (Nipro Medical Corporation, Osaka, Japan) was inserted into the trachea, using a fiber-optic light for guidance. After the fiber optic was pulled out, the clamped rubber tubing was connected onto the catheter to ventilate anesthesia into the animal. Once properly intubated, the subject was moved to a sterile field on the top of a warming pad, and the surgical site was wiped down with surgical scrub, ethanol, and surgical solution.

2.4. Cryo-infarction procedure

A cryo-probe made of a stainless-steel rod (316 SS, Arcelor Mittal) with 3 mm cross-sectional diameter was placed into liquid nitrogen. A thoracotomy was performed following a published protocol (van den Bos et al., 2005) through the fourth left intercostal space using a Rat Surgical Kit (Kent Scientific Corporation). After locating the heart and removing the pericardium, cryo-infarction was induced by touching the tip of the cryo-probe to the anterior left ventricular free wall for 10 s. Ice-cold PBS solution was then perfused through the heart to remove any blood from the inner chambers. The animal was sacrificed by removing the heart. Organ samples were fixed in 4% PFA overnight then switched to PBS before tissue sectioning. No post-operative mortality was observed or documented for any of the subjects used in this study.

2.5. Tissue sectioning

Hearts were placed in 30 % sucrose for dehydration and were bisected transversely from the apex of the heart. Samples were embedded into Neg-50 tissue medium and sectioned using a cryo-stat (ThermoFisher Scientific, Pittsburgh, PA) at 5 μm thickness (Roy et al., 2009). Tissue sections were collected onto uncoated glass slides and stored at −80 °C. Sections were then transferred to −20 °C overnight before any staining procedures described below.

2.6. Microscopic imaging

All H&E-, Gomori's trichrome-, and immunostained sections were visually examined under an Eclipse-Ni fluorescence microscope (Nikon Instruments Inc., Japan). A series of high–resolution images were then captured at 20x and 40x magnification with a CoolSNAP MYO camera (Photometrics, Tucson, AZ) and imported to the computer for image analysis.

2.7. H&E staining

Cardiac tissue sections were stained with hematoxylin and eosin following a modified, published protocol (Center, 2017). Slides were heated to 37 °C using a slide warmer (ThermoFisher Scientific, Pittsburgh, PA) for 20−30 min then submerged in 4% PFA for the 10 min. To remove tissue-embedding compounds, the sections were each rinsed twice in PBS, followed by a final rinse in a gentile tap water stream. Tissue was stained with Mayer's hematoxylin for 30 s, washed, then was dipped in a series of diluted ethanol concentrations. Sections were counterstained with alcoholic eosin, then were dehydrated through a second series of ethanol changes. Finally, tissue sections underwent three changes of Xylene for a minute each, and a coverslip was mounted on top of the section with xylene based mounting media. H&E stained samples were imaged at 40x magnification with a CoolSNAP MYO camera (Photometrics, Tucson, AZ) and imported to the computer for image-analysis and analyzed for cardiac muscle density, fiber length, and fiber curvature as described below (*2.7.1/.2/.3*).

2.7.1. Muscle density quantification

Myocardial density in tissue sections was calculated using ImageJ (National Institutes of Health, USA) through a color segmentation plug-in *ColorSegmentation_.jar* (described in supplementary information) (Sage, 2008). The pink-stained cytoplasm of cardiomyocytes was partitioned against the white background of the samples in RBG colored microscopic images. By splitting each color of interest in a channel, an algorithm segments the two pigmentation clusters and calculates the area occupied by each. This procedure was conducted on both sham and infarcted tissue sections, and an average area percentage of fiber muscle was calculated for comparison. The area to be measured was objectively random, and a total of twelve different sham and twelve different infarcted H&E micrographs were used to calculate average muscle density from each animal.

2.7.2. Fiber length quantification

Cardiac fiber length was calculated by drawing a line down the center of the muscle and recording the longest uninterrupted dimension. ImageJ was used for this task, after calibrating the software to the image's scale bar. The average fiber length was calculated for both the sham and infarcted groups for comparison. The average fiber length was calculated by measuring a total of fifty cardiomyocytes in each group from the same micrographs.

2.7.3. Fiber curvature quantification

A ratio of curvature (C) was determined by dividing the length along the contour of a cardiac fiber (Lc) to the length of the line segment between its two end-points (Ls), as expressed in Equation 1.

$$C = \frac{Lc}{Ls} \tag{1}$$

If Lc ~ Ls, then C1 and the fiber displays a linear character. On the other hand, if a fiber is wavy, a larger contour measurement is recorded, causing C > 1. The ratio cannot be less than 1, as theoretically Lc can never be less than Ls, since the shortest distance between two points is a straight line. After calibrating with the scale bar, ImageJ was used to measure Lc by drawing small line segments along the curve of the cardiac fibers and summing them. Ls was measured by drawing a line between the end-points of the same fiber. An average ratio was calculated and compared for both sham and experimental groups. About fifty measurements were used to calculate the average ratio of curvature for the cells.

2.8. Gomori's trichrome

A modified protocol was used to stain for collagen (ThermoScientific, 2012). Slides with cardiac tissue samples were placed in the slide warmer for 20−30 min and placed in Bouin's fluid at 56 °C for 30 min. Sections were rinsed in running tap water for 3−5 min until the yellow color is removed. They were subsequentially stained with Working Weigert's Iron Hematoxylin for 15 s and rinsed. Trichrome stain was applied for 15 min, moved to 1% acetic acid for 1 min, rinsed, and dehydrated in two changes of anhydrous alcohol for 1 min each. Finally, tissue sections underwent three changes of Xylene for a minute each, and coverslip was mounted on top of the section with xylene based mounting media. Samples that were stained with Gomori's Trichrome were imaged at 20x magnification with a CoolSNAP MYO camera (Photometrics, Tucson, AZ) and imported to the computer for image-analysis and analyzed for collagen, as described below (*2.8.1*).

2.8.1. Estimation of collagen

Collagen density in the tissue sections stained by Gomori's Trichrome was compared between sham and cryo-MI sections to understand the immediate effects of the Cryo-MI procedure on the collagen fibrils present in the cardiac muscle. To achieve this, the scale bar of microscopic images was set in ImageJ. The image was then split into red, green, and blue channels, and a threshold was set to remove any background. The area fraction of the collagen stain was then measured. Image area fractions were compared for sham and cryo-MI groups for comparison. The area to be measured was objectively random, and a total of twelve different sham and twelve different infarcted Gomori's stained micrographs were used to calculate average collagen expression, from each animal.

2.9. Immunohistochemistry

Slides with myocardial tissue sections were placed on a slide warmer, as done in Section 2.7. Tissues on slides were fixed with 4% PFA for 45 min, then rinse with 1X PBS three times for 10 min each. 0.1 % Sodium Borohydrate (NaBH₄) was added to the slides for 15 min and then rinsed thrice for 10 min in 1X PBS. Slides were blocked for 1 h at room temperature using a blocking solution (mentioned below), then rinsed 1X for 10 min in 1X PBS.

Primary antibody, a rabbit polyclonal anti-Connexin-43 antibody (Cell Signaling Technology Inc., Danvers, MA, USA Cat. # 3512S) was diluted at 1:400 dilution in antibody solution (as described below), which was then added to the slides and incubated overnight at 4 °C. After incubation, slides were rinsed with 1X PBS for 3 times. Secondary antibody, Alexa Fluor 594 goat anti-rabbit IgG (Invitrogen, Cat. #A-11037) at a concentration of 1:1000 were used. After one hour of incubation, the slides were washed with 1X PBS for 3 times, stained with DAPI (Cell Signaling Technology Inc., Danvers, MA, USA Cat. # 4083S; 20 mg/mL stock solution). DAPI was diluted at 1:50,000 in deionized water and incubated for 2−3 min. The tissues were rinsed with 1X PBS

for 3 times. Coverslips were mounted on slides using Fluoromount G (Electron Microscopy Sciences, Hatfield, PA). Blocking solution was prepared with 19 mL 1X phosphate buffer saline (PBS), 1 mL normal goat serum (NGS), 40 μL Triton X-100, and 2 μL 1000X NaAZide. The antibody solution was prepared with 19 mL 1X PBS, 1 mL NGS, and 2 μL 1000X NaAZide. Cardiac muscles are the positive control for CX-43. For negative control, the primary antibody was removed, and no background staining was observed. Samples that were immunochemically stained were used for comparing the expression of Cx-43 and nuclei (DAPI) in the Sham and cryo-MI tissue sections, as described below. Six-different fluorescent micrographs were used for Cx-43, and DAPI quantification for each tissue section investigated from sham and cryo-MI groups for comparison.

2.9.1. Nuclei and Cx-43 quantification

Representative colored fluorescent micrographs were converted into binary images on ImageJ, and a threshold to remove any background noise was set using negative control. Nuclei (DAPI) and areas of connexin-43 (Cx-43) expression were then counted using the software's *Analyze Particles* tool following a similar protocol (Papadopulos et al., 2007). The average number of nuclei and areas of fluoresced Cx-43 expression were calculated and compared. The outcome was presented in a graph format.

2.10. Statistical analysis

In order to carefully determine a sample size required to have a good chance of statistical significance with a given confidence level and a specified size of effect, a pilot analysis was performed using ANOVA to compare the expression of Cx-43 between sham and cryo-MI sample groups. The mean and standard error of the expression of Cx-43 could be deduced from published literature (Hawat et al., 2010), and we assumed a large effect size of 0.66 to detect the difference between control and experimental group effects on the end-point.

A power analysis for a comparison of these outcomes by experimental group (a power of 0.80, a large effect size of 0.66, and an alpha of 0.05 with adjustment for multiplicity) yielded a minimum sample size of 12; 6 for each group in sham and cryo-MI animals. Analysis of collected data was done following such a sampling design. Data collection occurred at strict predefined time points following written protocols, and outcomes were defined with precision. The means of data collection were not varied between experiments. Randomization was used were samples obtained from sham or cryo-MI induced tissue sources were assayed in no particular sequence. All instruments used in this study were calibrated periodically, well maintained, and administered with attention to protocol adherence.

The experimental set of animals underwent a thoracotomy and cryo-infarction. The control (sham) animals underwent a thoracotomy but were not cryo-infarcted. From these two groups, the procured hearts were sectioned in a manner that would allow for H&E, Gomori's tri-chrome, and immunofluorescence staining of each heart. Multiple images from different areas within each differently stained section were taken for analysis. Student's *t*-test (IBM SPSS, New York, USA) was used for statistical analysis between infarcted and sham groups for each quantitative study. All p-values where $p < 0.05$ were considered statistically significant.

3. Results and discussion

3.1. Surgical set-up

A schematic of the general surgical setup is illustrated in Fig. 1. The animal is intubated with an endotracheal tube and is placed supine on a surgical bed while anesthesia is maintained by the SomnoSuite. After a thoracotomy is performed to expose the heart, a cryo-probe is removed from liquid nitrogen and is touched to the LV wall.

3.2. Macroscopic characteristics post MI

A dark, brownish-red region was observed in the zone of cryo-infarction, as shown in Fig. 2A. This feature agrees with macroscopic findings in human coronary thrombosis-induced MI on relatively fresher infarcts as opposed to older ones, which exhibit a more grey or white color (White et al., 1936). An image of the cross-sectional tip of the cryo-probe is shown in Fig. 2B.

3.3. Muscle density

Representative sham and cryo-infarcted myocardium sections stained with H&E are illustrated in Fig. 3A and B, respectfully. Sham micrographs revealed the average area occupied by cardiac muscle to be $57 \pm 4\%$ as compared to $43 \pm 4\%$ negative space. On the other hand, the infarcted group expressed an average area of $42 \pm 6\%$ for myocardium and $58 \pm 6\%$ white background. A summary of this data is represented in Fig. 3C. Statistical analysis revealed a significant difference ($p = 2.28 \times 10^{-6}$) in the amount of cardiac muscle present between the two groups. A larger representative area for the sham and cryo-infarcted myocardium can be referenced in Supplementary Fig. 1. It is known that in transmural myocardial infarction, ischemia, and injury affect the entire thickness of the myocardial muscle, including the endocardium, myocardium, and epicardium (Saleh and Ambrose, 2018). This typically is the result of a complete occlusion of a large epicardial coronary artery
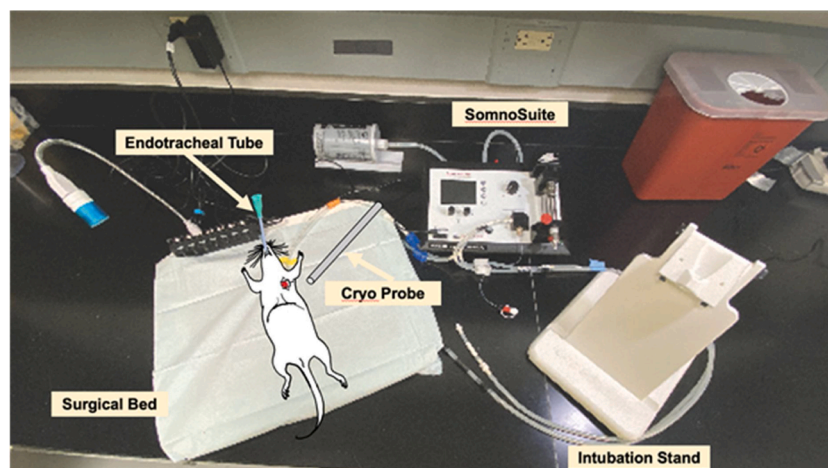

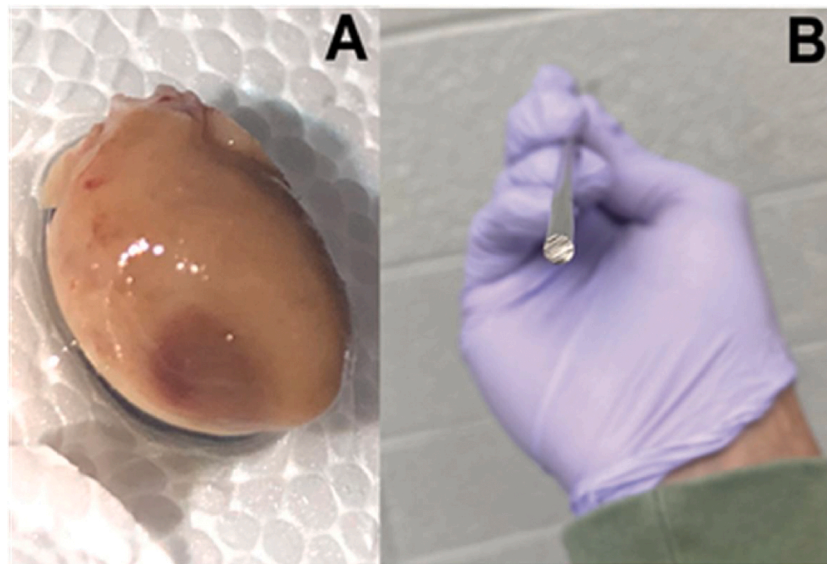**Fig. 1.** Experimental setup for inducing cryo-MI in a rat model.

Fig. 2. A zone of reddish-brown tissue appears on a rat heart (A) after cryo-induced MI with a 3-mm diameter stainless-steel cryo-probe (B).
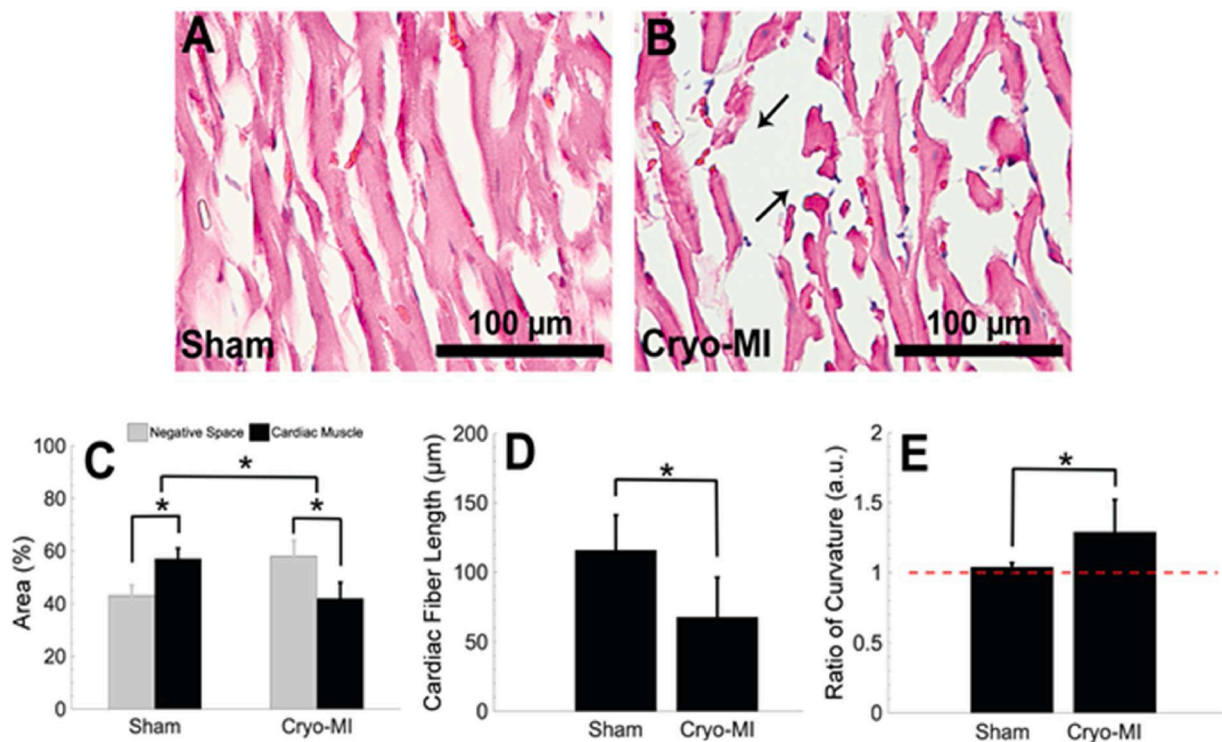

Fig. 3. Representative H&E stained myocardium tissue sections for sham (A) and cryo-infarcted (B) groups from n = 6 animals are displayed at 40X magnification. Cardiac muscle occupies more space in sham tissue sections than in infarcted ones (C). The average fiber length (Mean ± SD) is seen to decrease in cryo-infarcted samples (D) as well as an increase in waviness (E). Deviation from the red dashed line in E suggests fibers become wavy.

that is tied off in a LAD procedure or by a thrombus, resulting in decreased blood supply to all three layers of the heart muscle. Our findings are in agreement with the results obtained by LAD occlusion and confirm these observations as well. However, the significant advantage our technique poses compared to other published works is that the alteration in muscle density post cryo-MI is noticeable almost immediately in comparison to others' observations that are confirmed after 2–3 days of the procedure (van den Bos et al., 2005).

3.4. Fiber length

Cardiac fiber length was calculated by measuring the longest undisrupted distance of each muscle fiber. The average lengths displayed in Fig. 3D were found to be $116 \pm 25\,\mu m$ and $68 \pm 29\,\mu m$ for sham and infarcted groups, respectfully. Literature reports healthy cardiac fibers to be of about $60-100\,\mu m$ (Prabhu and Frangogiannis, 2016), values well within one standard deviation of our sham results. Muscle fragments introduced through the cryo-MI procedure had contributed smaller lengths, thereby decreasing the infarcted group's average. A

statistical significance ($p = 1.18 \times 10^{-14}$) was calculated. Introduction of cellular debris, either by apoptosis or cryo-infarction, are necessary to activate the inflammatory response that removes these fragments and makes room for compensatory extracellular matrix remodeling (Cleutjens et al., 1999; Prabhu and Frangogiannis, 2016). Our results directly contrast findings in the LAD setting, where it was observed that sham rats had a decreased fiber length as compared to LAD-infarcted rats (Yoshida et al., 2001). The difference in observations indicates LAD causes hypertrophy (Yoshida et al., 2001) of the cardiac fibers, a phenomenon not observed in our results.

3.5. Fiber curvature

An average curvature ratio of 1.04 ± 0.03 was calculated for healthy muscle fibers, while infarcted ones averaged 1.29 ± 0.23. There was a significant difference ($p = 3.15 \times 10^{-10}$) between both groups, as depicted in Fig. 3E. These values suggest that cardiac fibers in sham samples exhibited a more linear character as compared to those found in the infarcted group.

Introduction of wavy cardiac muscle fibers after an MI is a characteristic histopathologic feature that has been commonly described in the naturally-occurring MI (Fishbein et al., 1978); however, no literature in LAD ligation examines this effect for a direct comparison.

3.6. Collagen quantification

Representative sham and cryo-infarcted tissue sections stained with Gomori's trichrome are displayed in Fig. 4A and B, respectively. Collagen manifestation is visualized by the blue color. It can be seen that in Fig. 4A, the collagen staining is less evident. On the contrary, in Fig. 4B, the collagen staining appears to be more widespread, and distinct blue collagen fibers are present in the cardiac tissue sections.

The average collagen expression for sham sections was 5.7 ± 2.3 %, while cryo-MI sections averaged 25.5 ± 5.9 % with a statistical significance of $p = 8.3 \times 10^{-5}$. This result is in agreement with others' published works where the accumulation of diffuse collagenous fibers has been seen around the cardiac muscle bundles after an event of myocardial infarction (González et al., 2018). The difference in observed collagen is graphically represented in Fig. 4C. It is known that extracellular matrix remodeling, characterized by the deposition of a thick collagenous scar, occurs weeks after infarction. The data presented serves as a snapshot of histological collagen representation directly after infarction. Future studies will be conducted at time points downstream from infarction and compared to LAD ligation studies.

3.7. Nuclei and Cx-43 immunostaining

Representative immunoassayed myocardium sections are displayed

in Fig. 5A for sham, and Fig. 5B for infarcted groups. The total average number of nuclei for sham and cryo-MI samples of equivalent areas were 561 ± 88 and 412 ± 108, respectively. There was a significant difference ($p = 0.04$) between both groups. This information suggests cell death in cryo-infarcted cardiac tissue and corroborates results found in muscle density calculations. The number of areas that expressed Cx-43 was 552 ± 119 and 281 ± 135 for sham and cryo-MI groups, respectively, with a significant difference of $p = 0.03$ amongst them. In comparison with other published works, our results confirmed that there is significant death of cardiomyocytes indicated primarily by the reduced amount of DAPI staining, followed by disruption and disaggregation of the cardiac myocyte bundles (Cx-43) which is required for normal and healthy cardiac physiology and function (Kieken et al., 2009). Based on a published image reported by Kieken et al. (Kieken et al., 2009), we derived an average expression of Cx43 normalized to DAPI as 2.40 ± 0.28 for control and 1.88 ± 0.73 for LAD induced coronary occlusion in the animals studied. These trends in the change in Cx43 expression between and injury-groups are similar to the trends reported by us in Fig. 5C, D.

Furthermore, the presence of contraction bands (CB), which are characteristic of cell necrosis of myocardial cells, was also observed in cryo-MI induced tissue sections in comparison with controls (Supplementary Fig. 2).

4. Conclusion

This study offered a quantitative histological characterization of cryo-induced myocardial infarction in Sprague Dawley rats. We believe that this study is the first of its kind to perform extensive quantitative histopathological analysis to confirm the observational outcomes, also reported earlier by many groups (Bouchardy and Majno, 1974; van den Bos et al., 2005, Duerr2010). Hematoxylin and eosin staining was used to visualize cardiac tissue to measure the difference in muscle density, average fiber length, and fiber curvature for both sham and experimental group of animals. Overall, cryo-induced infarcts displayed cardiac fibers that were not as spatially abundant, shorter, and were distorted as compared to their sham counterparts. Gomori's trichrome showed an increased area of collagen expression in the infarcted tissue sections compared to the healthy sections.

Furthermore, immunohistochemical probing of DAPI and Cx-43 revealed more nuclei and intercellular Cx-43 expression in non-infarcted heart tissue. From these observations, a specific area of the cryo-infarct was induced and confirmed. These results imply that the cryo-infarction created in the rat animal model characterizes the anterior myocardial infarct with modest adverse collagen-based extracellular matrix remodeling and may be representative for infarcts seen in the clinic.

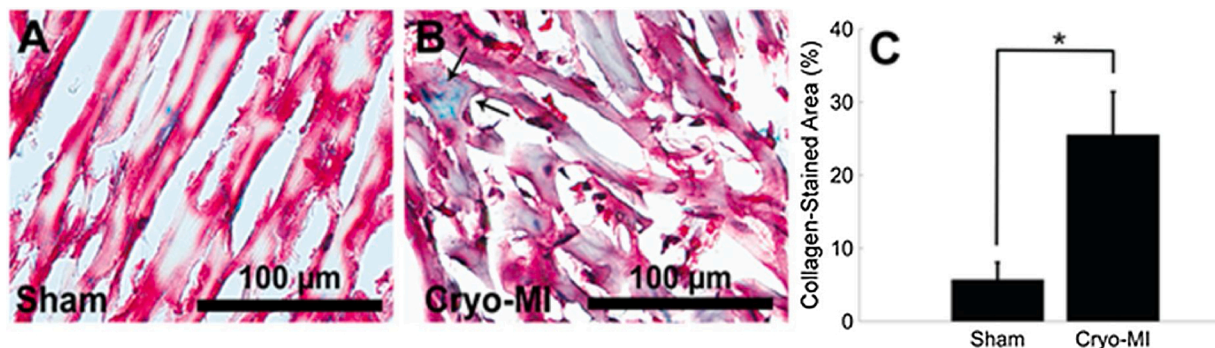In future studies, we hope to use this data to better design and

Fig. 4. Sections stained with Gomori's trichrome are shown for sham (A) and cryo-infarcted (B) samples from n = 6 animals. Green staining shows fewer collagen fibrils in sham sections, whereas the fibrils (pointed arrows) in infarcted tissue are more concentrated and widespread. The difference in the amount of collagen (Mean ± SD) measured among both groups was statistically significant (C).
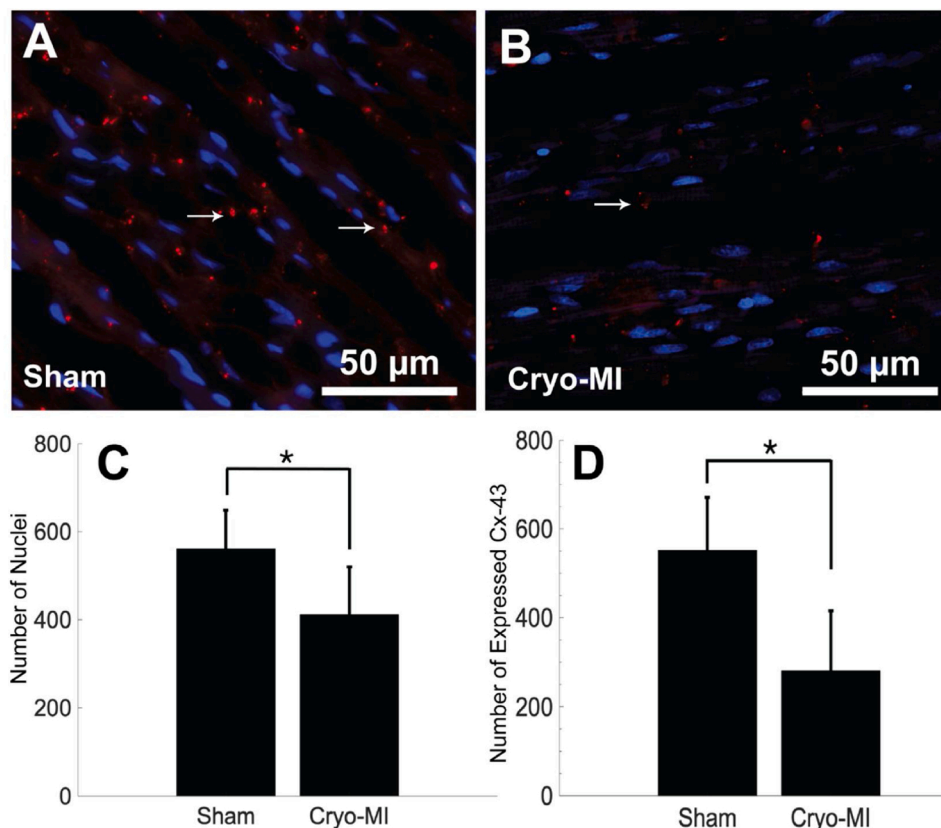
Fig. 5. Immunohistochemistry of myocardial tissue. Sham (A) and cryo-infarcted (B) sections are probed for expression of DAPI (blue) and Cx-43 (red) from n = 6 animals. Both the total average of nuclei (C) and Cx-43 (D) (Mean ± SD) were found to be greater in healthy myocardium than in infarcted tissue.

optimize a cardiac patch that can be surgically grafted into a defined and specific zone of infarcted myocardium (Anil Kumar et al., 2019). Furthermore, we aim to implement this technique at discrete timepoints after cryo-injury to study the histopathological development of the induced infarct. While LAD more closely resembles the pathophysiology of a naturally-occurring MI, the cryo-infarction technique produces a defined area of infarction that researchers may find as a valuable alternative in designing experimental protocols that minimize the variability in infarcted zones, and therefore do not require as many experimental iterations. This also has the additional benefit of reducing the number of animals used, and cryo-infarction is a relatively fast technique. One such example is the research and development of three-dimensional tissue-engineered cardiac grafts that aim to replace damaged and scarred myocardium (van den Bos et al., 2005; Anil Kumar et al., 2019). The ability to implant similar grafts in a controlled and reproducible manner using a technique such as in cryo-infarction will aid in their design and testing.

Furthermore the relevance of this study toward myocardial infarction is not limited. In one study, they compared the resultant infarct size in reperfusion therapy for acute myocardial infarction induced via invasive and non-invasive routes (Christian et al., 1992). Specifically the effects of non-invasive (similar to our study methods) versus invasive procedures such as the coronary artery occlusion in patients with acute myocardial infarction in relation to final infarct size was evaluated. In the invasive model, the resultant infarct was 70 % compared to the controls. In the noninvasive model, nearly identical results were obtained where the resultant area was 68 % compared to controls.

The cryo-injury model presented in this study holds the potential to advance interventions that aim to restore cardiac function or regeneration after MI, such as in the development of cellular myoplasty or cardiac tissue-engineered grafts. With this technique, grafts can be easily implanted into well-defined areas of the infarcted heart, and the repair

and integration process can be examined in an organized and repeated manner (van den Bos et al., 2005). Furthermore, this can be studied without explicit heart failure (van den Bos et al., 2005). The rodent animal model also introduces the possibility of implementing transgenic subjects (van den Bos et al., 2005). We have methodically laid out a quantitative histological analysis of cryo-induced MI in a rat model. We hope to use this data to better design and optimize a cardiac patch that can be surgically grafted onto the infarcted myocardium.

Data availability statement

Raw data available upon request from the corresponding author.

Funding sources

CRediT authorship contribution statement

Matthew Alonzo: Writing - original draft, Writing - review & editing. **Monica Delgado:** Data curation, Writing - original draft, Software, Validation. **Carol Cleetus:** Writing - original draft. **Shweta Anil Kumar:** Writing - original draft, Visualization, Investigation, Data curation, Writing - review & editing. **Vikram Thakur:** Writing - original draft, Visualization, Investigation, Data curation. **Munmun Chattopadhyay:** Conceptualization; Supervision, Mentoring and Guidance: Writing-

Original and final drafts, reviewing and editing. **Binata Joddar:** Conceptualization; Supervision, Mentoring and Guidance: Writing-Original and final drafts, reviewing and editing.

Declaration of Competing Interest

The authors report no declarations of interest.

Appendix A. Supplementary data

Supplementary material related to this article can be found, in the online version, at doi:https://doi.org/10.1016/j.acthis.2020.151624.

References

Anil Kumar, S., Alonzo, M., Allen, S.C., Abelseth, L., Thakur, V., Akimoto, J., Ito, Y., Willerth, S.M., Suggs, L., Chattopadhyay, M., Joddar, B., 2019. A visible light-cross-linkable, fibrin–gelatin-based bioprinted construct with human cardiomyocytes and fibroblasts. ACS Biomater. Sci. Eng. 5 (9), 4551–4563. https://doi.org/10.1021/acsbiomaterials.9b00505.

Bouchardy, B., Majno, G., 1974. Histopathology of early myocardial infarcts: a new approach. Am. J. Pathol. 74 (2), 301–330.

Choo, E.H., Chang, K., Lee, K.Y., Lee, D., Kim, J.G., Ahn, Y., Kim, Y.J., Chae, S.C., Cho, M. C., Kim, C.J., Kim, H.S., 2019. Prognosis and predictors of mortality in patients suffering myocardial infarction with non-obstructive coronary arteries. J. Am. Heart Assoc. 8 (14) https://doi.org/10.1161/JAHA.119.011990 e011990.

Christian, T.F., Schwartz, R.S., Gibbons, R., 1992. Determinants of infarct size in reperfusion therapy for acute myocardial infarction. Circulation 86 (1), 81–90. https://doi.org/10.1161/01.CIR.86.1.81.

Ciulla, M.M., Paliotti, R., Ferrero, S., Braidotti, P., Esposito, A., Gianelli, U., Busca, G., Cioffi, U., Bulfamante, G., Magrini, F., 2004. Left ventricular remodeling after experimental myocardial cryoinjury in rats. J. Surg. Res. 116 (1), 91–97. https://doi.org/10.1016/j.jss.2003.08.238.

Cleutjens, J.P., Blankesteijn, W.M., Daemen, M.J., Smits, J.F., 1999. The infarcted myocardium: simply dead tissue, or a lively target for therapeutic interventions. Cardiovasc. Res. 44 (2), 232–241. https://doi.org/10.1016/S0008-6363(99)00212-6.

Duerr, G.D., Elhafi, N., Bostani, T., Ellinger, J., Swieny, L., Kolobara, E., Welz, A., Dewald, O., 2010. Comparison of myocardial remodeling between cryoinfarction and reperfused infarction in mice. J. Biomed. Biotechnol. 2011 https://doi.org/10.1155/2011/961298.

Fishbein, M.C., Maclean, D., Maroko, P.R., 1978. The histopathologic evolution of myocardial infarction. Chest 73 (6), 843–849. https://doi.org/10.1378/chest.73.6.843.

González, A., Schelbert, E.B., Díez, J., Butler, J., 2018. Myocardial interstitial fibrosis in heart failure: biological and translational perspectives. J. Am. Coll. Cardiol. 71 (15), 1696–1706. https://doi.org/10.1016/j.jacc.2018.02.021.

Hasenfuss, G., 1998. Animal models of human cardiovascular disease, heart failure and hypertrophy. Cardiovasc. Res. 39 (1), 60–76. https://doi.org/10.1016/S0008-6363(98)00110-2.

Hawat, G., Benderdour, M., Rousseau, G., Baroudi, G., 2010. Connexin 43 mimetic peptide Gap26 confers protection to intact heart against myocardial ischemia injury. Pflügers Arch.-Eur. J. Physiol. 460 (3), 583–592. https://doi.org/10.1007/s00424-010-0849-6.

Kieken, F., Mutsaers, N., Dolmatova, E., Virgil, K., Wit, A.L., Kellezi, A., Hirst-Jensen, B. J., Duffy, H.S., Sorgen, P.L., 2009. Structural and molecular mechanisms of gap junction remodeling in epicardial border zone myocytes following myocardial infarction. Circ. Res. 104 (9), 1103–1112. https://doi.org/10.1161/CIRCRESAHA.108.190454.

Klocke, R., Tian, W., Kuhlmann, M.T., Nikol, S., 2007. Surgical animal models of heart failure related to coronary heart disease. Cardiovasc. Res. 74 (1), 29–38. https://doi.org/10.1016/j.cardiores.2006.11.026.

Papadopulos, F., Spinelli, M., Valente, S., Foroni, L., Orrico, C., Alviano, F., Pasquinelli, G., 2007. Common tasks in microscopic and ultrastructural image analysis using ImageJ. Ultrastruct. Pathol. 31 (6), 401–407. https://doi.org/10.1080/01913120701719189.

Prabhu, S.D., Frangogiannis, N.G., 2016. The biological basis for cardiac repair after myocardial infarction: from inflammation to fibrosis. Circ. Res. 119 (1), 91–112. https://doi.org/10.1161/CIRCRESAHA.116.303577.

Reichert, K., Colantuono, B., McCormack, I., Rodrigues, F., Pavlov, V., Abid, M.R., 2017. Murine left anterior descending (LAD) coronary artery ligation: an improved and simplified model for myocardial infarction. JoVE (J. Visual. Exp.) 122. https://doi.org/10.3791/55353 e55353.

Richardson, W.J., Clarke, S.A., Quinn, T.A., Holmes, J.W., 2011. Physiological implications of myocardial scar structure. Compr. Physiol. 5 (4), 1877–1909. https://doi.org/10.1002/cphy.c140067.

Roy, S., Khanna, S., Hussain, S.R.A., Biswas, S., Azad, A., Rink, C., Gnyawali, S., Shilo, S., Nuovo, G.J., Sen, C.K., 2009. MicroRNA expression in response to murine myocardial infarction: miR-21 regulates fibroblast metalloprotease-2 via phosphatase and tensin homologue. Cardiovasc. Res. 82 (1), 21–29. https://doi.org/10.1093/cvr/cvp015.

Rusu, M., Hilse, K., Schuh, A., Martin, L., Slabu, I., Stoppe, C., Liehn, E.A., 2019. Biomechanical assessment of remote and postinfarction scar remodeling following myocardial infarction. Sci. Rep. 9 (1), 1–13. https://doi.org/10.1038/s41598-019-53351-7.

Sage, D., 2008. Color Segmentation: ImageJ Plug-in to Cluster Color Pixel Driven by the User Input. http://bigwww.epfl.ch/sage/soft/colorsegmentation/.

Saleh, M., Ambrose, J.A., 2018. Understanding myocardial infarction. F1000Research 7. https://doi.org/10.12688/f1000research.15096.1.

Schwarzer, M., 2016. Chapter 8 - Models to Investigate Cardiac Metabolism, The Scientist's Guide to Cardiac Metabolism. Academic Press, pp. 103–122. https://doi.org/10.1016/B978-0-12-802394-5.00008-X.

ThermoScientific, 2012. Thermo Scientific Richard-allan Scientific Chromaview – Advanced Testing Gomori's Trichrome Stain – Green Collagen. Instructions for Use.

van den Bos, E.J., Mees, B.M., de Waard, M.C., de Crom, R., Duncker, D.J., 2005. A novel model of cryoinjury-induced myocardial infarction in the mouse: a comparison with coronary artery ligation. Am. J. Physiol.-Heart Circ. Physiol. 289, 3. https://doi.org/10.1152/ajpheart.00111.2005. H1291-H1300.

Vunjak-Novakovic, G., Lui, K.O., Tandon, N., Chien, K.R., 2011. Bioengineering heart muscle: a paradigm for regenerative medicine. Annu. Rev. Biomed. Eng. 13, 245–267. https://doi.org/10.1146/annurev-bioeng-071910-124701.

White, P.D., Mallory, G.K., Salcedo-Salgar, J., 1936. The speed of healing of myocardial infarcts. Trans. Am. Clin. Climatol. Assoc. 52, 97. https://doi.org/10.1016/s0002-8703(39)90845-8.

Xue, M., Jackson, C.J., 2015. Extracellular matrix reorganization during wound healing and its impact on abnormal scarring. Adv. Wound Care (New Rochelle) 4 (3), 119–136. https://doi.org/10.1089/wound.2013.0485.

Yoshida, H., Tanonaka, K., Miyamoto, Y., Abe, T., Takahashi, M., Anand-Srivastava, M. B., Takeo, S., 2001. Characterization of cardiac myocyte and tissue β-adrenergic signal transduction in rats with heart failure. Cardiovasc. Res. 50 (1), 34–45. https://doi.org/10.1016/S0008-6363(01)00203-6.